Author's personal copy

Journal of Neuroscience Methods 177 (2009) 194–198

Contents lists available at ScienceDirect

Journal of Neuroscience Methods

journal homepage: www.elsevier.com/locate/jneumeth

Short communication

What is the real shape of extracellular spikes?

R. Quian Quiroga *

Department of Engineering, University of Leicester, LE1 7RH Leicester, UK

ARTICLE INFO

Article history:
Received 4 September 2007
Received in revised form
24 September 2008
Accepted 30 September 2008

Keywords:
Spikes
Spike detection
Spike sorting
Filtering
Single cell recordings

ABSTRACT

We show that the standard filters used for on-line spike detection in most hardware acquisition systems introduce distortions in the recorded spike shapes. This is because on-line spike detection is done after band pass filtering the data with causal filters. As illustrated with three clusters of spike shapes from a real single cell recording in a human subject, causal filtering can create a spurious negative rebound and a smooth looking appearance of the spikes. We also show that these filtering distortions can make artifacts look similar to real spikes.

© 2008 Elsevier B.V. All rights reserved.

1. Introduction

A gold standard in neuroscience is to study how neurons, recorded intracranially in different brain areas, behave upon different experimental conditions. For this, high impedance electrodes with a diameter of a few microns are introduced in animal brains and the activity of neurons close-by the electrode tip, within a neighbourhood of about 50–100 μm (Henze et al., 2000), is recorded extracellularly.

To a first approximation, neurons are either in a resting state or firing action potentials, or 'spikes'. These are a couple of milliseconds long and should not be confused with electroencephalographic spikes, typical of epileptic activity. Spikes are very tiny in the raw data, which is dominated by low frequency activity. Therefore, the standard first step in the analysis of neuronal recordings is to band pass filter the signal. After filtering, spikes are easily visualized on top of background noisy activity and can be detected, for example, by using an amplitude threshold (see Fig. 3). Although most algorithms use band pass filtering and amplitude thresholding for spike detection (Quian Quiroga, 2007), we note that it is in principle possible to detect the spikes without the use of band pass filtering, for example using template matching, wavelets or derivatives of the signal (Abeles and Goldstein, 1977; Nenadic and Burdick, 2005).

Each neuron fires spikes of a particular shape, based mainly on the morphology of its dendritic tree, the distance and orientation relative to the recording electrode, the distribution of ionic channels and the inhomogeneity of the extracellular medium (Gold et al., 2006). These differences in spike shapes can, in principle, disentangle which spike corresponds to which of the recorded neurons using 'spike sorting' algorithms (Lewicki, 1998; Harris et al., 2000; Quian Quiroga et al., 2004; Quian Quiroga, 2007). Much emphasis has been given to the development of optimal spike detection and sorting algorithms in the last years (Lewicki, 1998). However, the typical first basic step for the analysis of neuronal recordings, namely, band pass filtering the data, has been largely overlooked. In this study we will show how commonly used filter designs, as implemented in most hardware acquisition systems, introduce dramatic distortions in the spike shapes. This limitation is basically given by the use of causal filters, which are used for on-line processing of the data. There are a few applications where the actual shape of the recorded spikes may be critical. For example, filtering distortions should be taken into account – or removed if possible – in modeling studies of extracellular action potentials (e.g. Gold et al., 2006). Otherwise, distorted spike shapes may lead to an incorrect estimation of the model or its parameters. Filtering artifacts may also compromise the distinction between the spikes of pyramidal and inhibitory neurons (Csicsvari et al., 1999) or interpretations about the relationship between intra- and extra-cellular action potentials (Henze et al., 2000).

2. Materials and methods

2.1. Subject and recordings

To illustrate the effect of filtering distortions of the spike shapes a half an hour recording from the medial temporal lobe of a human

* Tel.: +44 116 252 2314; fax: +44 116 252 2619.
E-mail address: rqqg1@le.ac.uk.

0165-0270/$ – see front matter © 2008 Elsevier B.V. All rights reserved.
doi:10.1016/j.jneumeth.2008.09.033

Author's personal copy

subject will be used. The subject had pharmacologically intractable epilepsy and was implanted with intracranial electrodes for clinical reasons. Besides the standard low impedance contacts for recording intracranial EEG at different locations, each intracranial electrode probe had a total of 9 micro-wires at its end, 8 active recording channels and 1 reference to record single-neuron activity (Fried et al., 1997). The differential signal from the micro-wires was amplified and sampled at 28 kHz (Quian Quiroga et al., 2005). Before sampling, the signal was filtered between 1 and 9000 Hz with a Butterworth filter (filter rolloff 12 dB per Octave). Note that the cutoff frequencies of this filter are far from the frequency range of the spikes (~300–3000 Hz). Therefore for this frequency range the phase response is linear and the filter does not introduce distortions in the spike shapes.

Spike detection and sorting were performed with the software "Wave_Clus" (Quian Quiroga et al., 2004), as described in the Supplementary Material.

2.2. Filtering implementations

In this study we used elliptic filters, which are recursive (or infinite impulse response, IIR) filters with equiripple approximation in both the passband and the stopband and have the sharpest passband–stopband transition for a given order (Oppenheim, 1975; Lynn and Fuerst, 1989). The main advantage of elliptic filters – and other recursive implementations – over non-recursive (or Finite Impulse Response, FIR) designs is their computational economy. In fact, they usually have very few coefficients and are therefore easy to be implemented on-line. Another important difference between IIR and FIR filters is that the later ones are almost entirely restricted to discrete implementations and consequently they are not suitable for filtering a continuous signal (e.g. to avoid aliasing) before it is sampled (Oppenheim, 1975). For these reasons, most acquisition systems for single-cell recordings use IIR implementations (e.g. Butterworth, Elliptic). The major disadvantage of recursive IIR filters is that they are causal (i.e. each datapoint is evaluated from previous ones) and cannot provide in general a linear phase response. This may lead to filtering distortions, as we describe below.

To show the effect of filtering distortions in the shape of the spikes, we used three different implementations of a fourth order elliptic filter: (i) a *noncausal* filter in the range 300–3000 Hz; (ii) a *causal* filter in the range 300–3000 Hz; and (iii) a *causal* filter in the range 600–3000 Hz. The causal implementations were obtained with the matlab function 'filter' and for the noncausal ones we used the function 'filtfilt', which filters the data in the forward and in the reverse direction, thus giving a zero phase lag. Although the filtering distortions we will show here were obtained with elliptic filters, these results also apply to other recursive filtering implementations used by single-cell recording systems.

Fig. 1 shows the magnitude and phase response of a (causal) fourth order elliptic bandpass filter between 300 and 3000 Hz. The filter was implemented with two sets of 5 coefficients. As expected, there is a strong attenuation for frequencies below 300 Hz and frequencies above 3000 Hz. Moreover, there is a non-linear dependence of the phase with the frequency. To illustrate the effect of such a non-linear phase response, in Fig. 2 we show how a causal and a noncausal filter implementation distorts a single pulse. In both cases we used the elliptic filter described above with the functions 'filter' and 'filtfilt', respectively. The causal filter introduces an asymmetric distortion with a marked spurious negative peak and a slow rebound. The noncausal filter gives a signal that is more similar to the original pulse, with only smoother and symmetric differences together with small ripples.

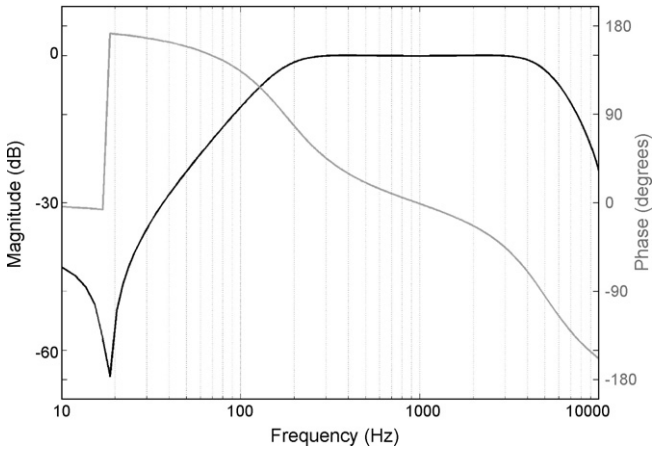

Fig. 1. Magnitude and phase response of a fourth order band-pass elliptic filter between 300 and 3000 Hz.

3. Results

Fig. 3a shows the first 10 s of the continuous data, as recorded from the electrode after amplification. The data has an overall amplitude of about 400 μV and it is mainly dominated by low frequency activity between 1 and 2 Hz. Spikes have an amplitude between 50 and 150 μV (SNR between 0.01 and 0.15) and are barely visible in this recording. However, they become clear after band pass filtering, as seen in Fig. 3b. In this case the spikes have an amplitude between 30 and 130 μV with a noise level of about 20 μV (SNR between 2 and 50). Note that it would be practically impossible to identify the spikes from the data without filtering. On the contrary, it is not difficult to detect them after band pass filtering, for example, using an amplitude threshold (horizontal line).

From the recording of Fig. 3 it was possible to identify 3 clusters after spike sorting, as shown in the Supplementary Material. Fig. 4a shows the 3 clusters of spike shapes, where the data was filtered using an noncausal filter between 300 and 3000 Hz (this is the default option of Wave_clus). The distinguishing characteristic of noncausal designs is that they filter each value x_i using a window W centered on it, $W = \{x_{i-T/2}, \ldots, x_{i+T/2}\}$, where T is the length of the filter. Notably, this type of spike shapes is very similar to the

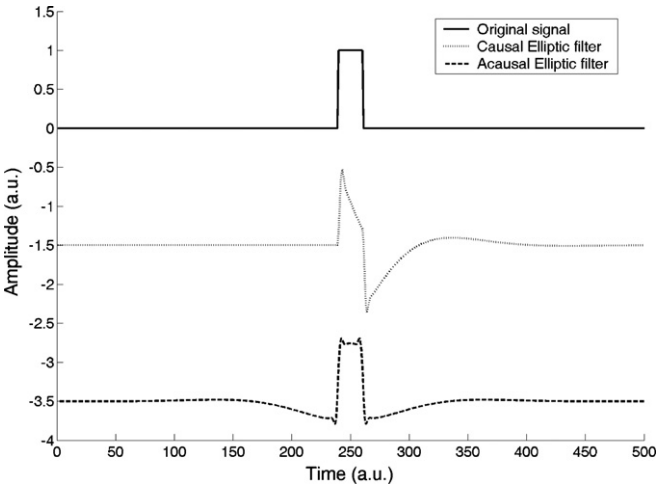

Fig. 2. Example of filtering distortions introduced by causal filters. The causal elliptic filter introduces asymmetric distortions and the filtered signal barely resembles the original pulse. Distortions are smaller with the noncausal implementation of the same elliptic filter.

Author's personal copy

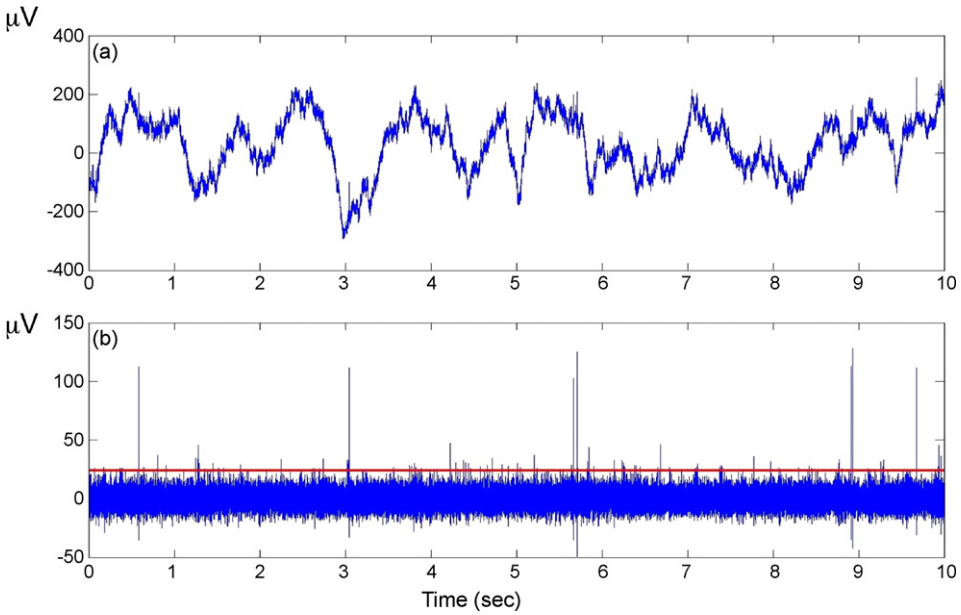

Fig. 3. (a) Ten seconds of a continuous recoding from a microwire in the medial temporal lobe of a human subject. The raw data is dominated by low frequency activity and it is very difficult to visualize the spikes. (b) The same recording after band pass filtering. Note that spikes can now be easily detected with an amplitude threshold (horizontal line).

ones reported with realistic simulations of extracellularly recorded action potentials (Gold et al., 2006).

Fig. 4b discloses the same clusters but in this case the spikes were detected using a causal filter between 300 and 3000 Hz. Causal filter implementations evaluate each datapoint x_i using a window that considers only the previous data, $W = \{x_{i-T}, \ldots, x_i\}$. As a consequence, causal filters introduce phase distortions, i.e.: delays that are a nonlinear function of the frequency (Oppenheim, 1975; Lynn and Fuerst, 1989). This is reflected in a distorted shape of the spikes. Note in particular the large negative rebound of the 3 clusters of

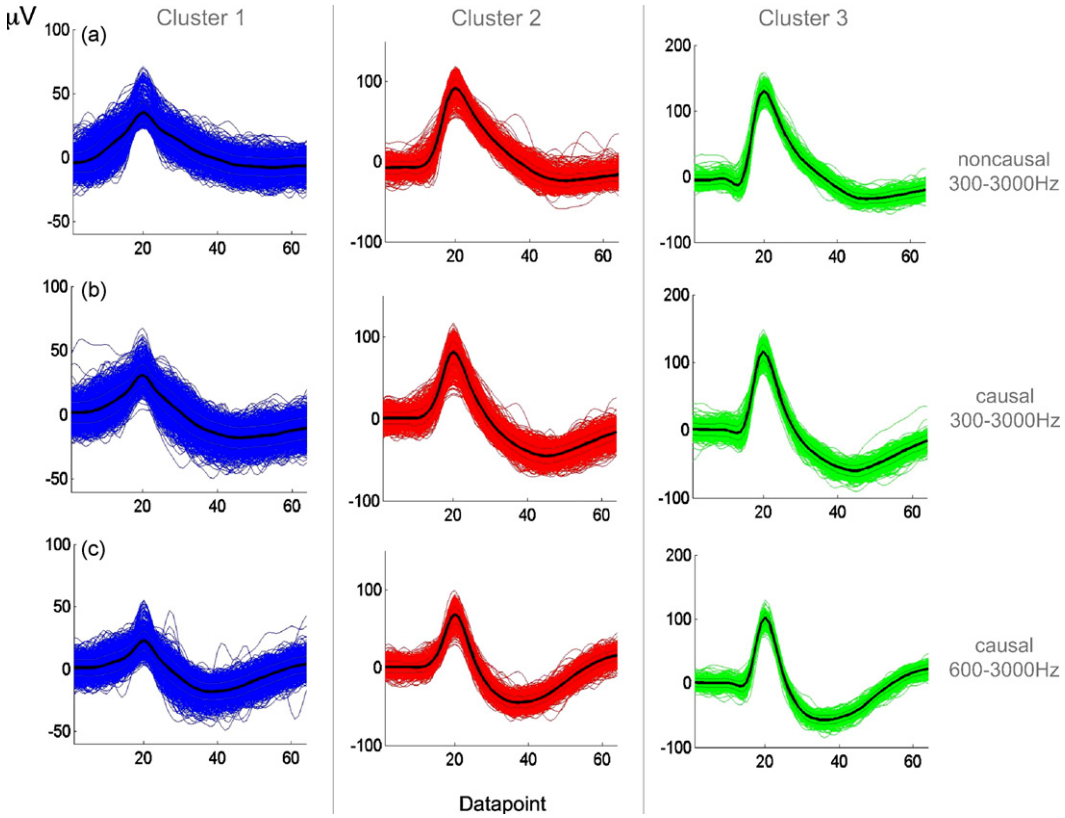

Fig. 4. The 3 clusters of spike shapes obtained from the previous figure, detected using different filters: (a) noncausal filter between 300 and 3000 Hz, (b) causal filter between 300 and 3000 Hz and (c) causal filter between 600 and 3000 Hz. Note the distortions of the spike shapes introduced by the causal filters.

Author's personal copy

Table 1
Root mean square distance (RMS) between the average spike shapes of Fig. 4 for the 3 different filtering implementations. Filters I, II and III correspond to the filters of Fig. 4a–c, respectively.

	Filter I	Filter II	Filter III
RMS_{12}	21.92	20.93	16.91
RMS_{13}	33.68	32.54	27.11
RMS_{23}	12.65	12.28	10.77

spikes that were not present in Fig. 4a. This effect is more marked when a higher cutoff frequency is used. Fig. 4c shows the results with a causal filter between 600 and 3000 Hz. This range and even higher values of the lower cutoff frequency are commonly used for the analysis of extracellular recordings (see e.g. Harris et al., 2000). Besides the spurious rebound, these spike shapes look much smoother than the ones of Fig. 4a. Similar distortions of the spike shapes were obtained with causal Butterworth or Chebyshev filters (not shown).

Next, we used a root mean square distance (RMS) to quantify the difference between the 3 clusters of spike shapes, for each of the 3 filtering implementations. For example, the distance between the average spike shapes of clusters 1 and 2 was defined as: $RMS_{12} = \sqrt{\frac{1}{N}\sum_{i=1}^{N}(x_{1i} - x_{2i})^2}$, where $N = 64$ is the number of datapoints of each average spike. Results for all 3 filtering implementations are shown in Table 1. Clearly, cluster 2 and cluster 3 are more similar to each other in comparison to cluster 1 and consequently their distance is smaller for all filtering implementations. Interestingly, all distances are larger for the noncausal filter of Fig. 4a and smaller for the more distorted spike shapes of Fig. 4c. So, although it was possible to detect the 3 clusters with all filtering implementations, the distance between them was largest with the non-distorted spike shapes.

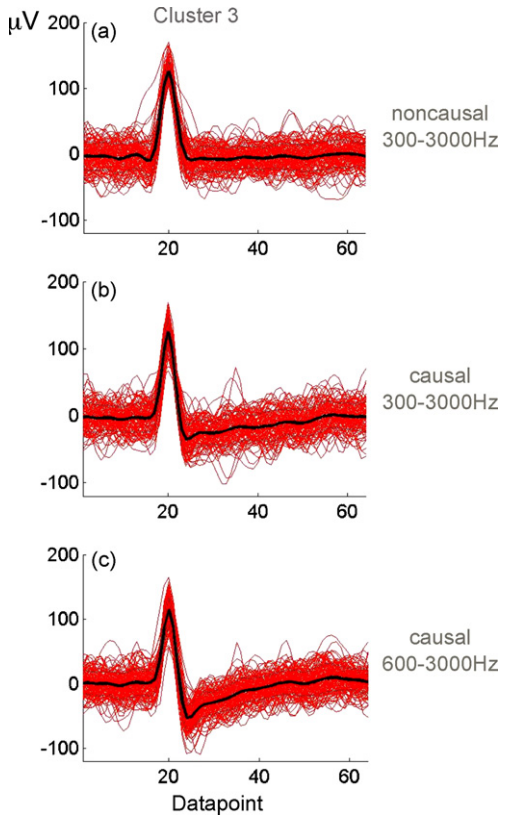

Fig. 5. A pulse artifact detected with the same filter settings of the previous figure. Note that the causal filter distorts the shape of the artifact and makes it look similar to a real spike.

Causal filters not only distort the spike shapes, but can also change the appearance of artifacts and make them look similar to real neural data. This is illustrated in Fig. 5 with an artifact that is clearly recognizable due to its sharp and symmetric appearance (Fig. 5a). As illustrated in Fig. 5b and especially in Fig. 5c, the use of causal filtering introduces asymmetric distortions with a negative rebound and a slow return to baseline. Note that one of the clearest indications of the artifact in Fig. 5a, its symmetric appearance, is lost and the distorted artifact may be confused with a real spike.

4. Discussion

In this study we showed how spike shapes can be seriously distorted by the causal filters commonly used for on-line spike detection. We illustrated this effect with elliptic filters, but similar results were obtained with Butterworth or Chebyshev causal filters. The use of causal implementations for band pass filtering is not arbitrary, but rather due to practical limitations. Indeed, hardware acquisition systems usually record only the times and shapes of spikes crossing an amplitude threshold set by the user, rather than the whole continuous data coming from the microwires. This is mainly for two reasons. First, although the recording of the continuous data allows the use of noncausal filters without shape distortions offline, it demands large storage capacity and sophisticated data processing. This is particularly critical if several channels are recorded simultaneously, which is becoming a more common practice for the study of complex brain processes that are reflected by the activity of large population of neurons (Brown et al., 2004; Buzsaki, 2004). For example, it is necessary to store and process over 10 GB of data for a 1 h recording session with the 64-channel equipment used to record the data presented in this study. Second, although current hardware capabilities and recent algorithmic implementations make the analysis of such volumes of data feasible, it is still desirable to get feedback of the neuronal responses during the recording session. This is particularly critical for closed-loop systems, where an animal gets on-line feedback on its performance in a given task, for example, for the development of prostheses directly controlled by neuronal activity (Andersen et al., 2004). We remark that single-cell recording systems use IIR recursive (i.e. causal) filters, such as Butterworth or elliptic because: (i) they have very few coefficients and are therefore easy to be implemented online, and (ii) FIR filters are almost entirely restricted to discrete implementations, thus not being suitable for filtering the signal before sampling, for example to avoid aliasing (Oppenheim and Schafer, 1975).

From the previous discussion, there seems to be a compromise between: (i) recording the on-line detected but distorted spike shapes to get feedback during the session, and (ii) recording the whole continuous data for optimal but off-line spike detection and sorting. However, it should be in principle possible to implement short buffers in the acquisition systems that will allow noncausal filtering, introducing only small processing delays. For example, the elliptic band pass filter we used in this study for spike detection was implemented with only two sets of 5 coefficients. Then, for the typical sampling frequencies of 10–50 kHz of single cell acquisition systems, a forward and reverse filtering – as implemented in the Matlab function 'filtfilt' – would give a noncausal implementation with a delay of only a fraction of a millisecond. This buffer could be implemented immediately after an antialiassing IIR filter and

Author's personal copy

digitization. Note that although the antialiassing filter is causal, its cutoff frequency could be set far from the frequency content of the spikes, thus not distorting their shapes. Such a set up would provide the best scenario with non-distorted spike shapes and nearly on-line performance.

Although in principle one can just record the firing of neurons without caring much how their spikes look like, there are some applications for which the actual spike shapes are important. First, this information is critical to design realistic models of extracellular action potentials (Gold et al., 2006). Interestingly, the spikes modeled by Gold and colleagues look very similar to the ones shown in this study without filtering distortions. Second, it is important to know the real spike shapes to study the relationship between intra- and extra-cellular action potentials (Henze et al., 2000; Smith and Mtetwa, 2007). Third, differences in spike shapes have been proposed to distinguish between pyramidal and inhibitory neurons (Csicsvari et al., 1999). Finally, even if not necessary for the actual results of a given experiment, it is interesting to know how the spikes we use for such computations really look like.

Acknowledgements

This work was supported by EPSRC and the Life Sciences Interface Programme, MRC and the Royal Society.

Appendix A. Supplementary data

Supplementary data associated with this article can be found, in the online version, at doi:10.1016/j.jneumeth.2008.09.033.

References

Andersen RA, Burdick JW, Musallam S, Pesaran B, Cham JG. Cognitive neural prosthetics. Trends Cogn Sci 2004;8:486–93.
Abeles M, Goldstein Jr M. In: Multispike train analysis; 1977. p. 762–73.
Brown EN, Kass RE, Mitra PP. Multiple neural spike train data analysis: state-of-the-art and future challenges. Nat Neurosci 2004;7:456–61.
Buzsaki G. Large-scale recording of neuronal ensembles. Nat Neurosci 2004;7:446–51.
Csicsvari J, Hirase H, Czurkó A, Mamiya A, Buzsáki G. Oscillatory coupling of hippocampal pyramidal cells and interneurons in the behaving rat. J Neurosci 1999;19:274–87.
Fried I, MacDonald KA, Wilson CL. Single neuron activity in human hippocampus and amygdala during recognition of faces and objects. Neuron 1997;18:753–65.
Gold C, Henze DA, Koch C, Buzsaki G. On the origin of the extracellular action potential waveform: a modeling study. J Neurophysiol 2006;95:3113–28.
Harris KD, Henze DA, Csicsvari J, Hirase H, Buzsaki G. Accuracy of tetrode spike separation as determined by simultaneous intracellular and extracellular measurements. J Neurophysiol 2000;84:401–14.
Henze DA, Borhegyi Z, Csicsvari J, Mamiya A, Harris KD, Buzsaki G. Intracellular features predicted by extracellular recordings in the hippocampus in vivo. J Neurophysiol 2000;84:390–400.
Lewicki M. A review of methods for spike sorting: the detection and classification of neural action potentials. Network: Comput Neural Systems 1998;9:R53–78.
Lynn PA, Fuerst W. Introductory digital signal processing with computer applications. John Wiley & Sons, Inc; 1989.
Nenadic Z, Burdick JW. Spike detection using the continuous wavelet transform. IEEE Trans Biomed Eng 2005;52:74–87.
Oppenheim AV, Schafer RW. Digital signal processing. Prentice Hall, New Jersey; 1975.
Quian Quiroga R, Nadasdy Z, Ben-Shaul Y. Unsupervised spike detection and sorting with wavelets and superparamagnetic clustering. Neural Comp 2004;16:1661–87.
Quian Quiroga R, Reddy L, Kreiman G, Koch C, Fried I. Invariant visual representation by single neurons in the human brain. Nature 2005;435:1102–7.
Quian Quiroga R. Spike sorting. Scholarpedia 2007;2(12):3583.
Smith LS, Mtetwa N. A tool for synthesizing spike trains with realistic interference. J Neurosci Methods 2007;159:170–80.